PHYSICAL REVIEW E **69**, 066204 (2004)

Semiclassical approximations based on complex trajectories

A. D. Ribeiro,[1] M. A. M. de Aguiar,[1] and M. Baranger[2,3]
[1]*Instituto de Física "Gleb Wataghin," Universidade Estadual de Campinas, Unicamp, 13083-970, Campinas, São Paulo, Brazil*
[2]*Center for Theoretical Physics, Laboratory for Nuclear Science and Department of Physics, Massachusetts Institute of Technology, Cambridge, Massachusetts 02139, USA*
[3]*Physics Department, University of Arizona, Tucson, Arizona 85719, USA*
(Received 5 January 2004; published 4 June 2004)

The semiclassical limit of the coherent state propagator $\langle \mathbf{z}''|e^{-i\hat{H}T/\hbar}|\mathbf{z}'\rangle$ involves complex classical trajectories of the Hamiltonian $\tilde{H}(\mathbf{u},\mathbf{v})=\langle \mathbf{v}|\hat{H}|\mathbf{u}\rangle$ satisfying $\mathbf{u}(0)=\mathbf{z}'$ and $\mathbf{v}(T)=\mathbf{z}''^*$. In this work we study mostly the case $\mathbf{z}'=\mathbf{z}''$. The propagator is then the return probability amplitude of a wave packet. We show that a plot of the exact return probability brings out the quantal images of the classical periodic orbits. Then we compare the exact return probability with its semiclassical approximation for a soft chaotic system with two degrees of freedom. We find two situations where classical trajectories satisfying the correct boundary conditions must be excluded from the semiclassical formula. The first occurs when the contribution of the trajectory to the propagator becomes exponentially large as $\hbar$ goes to zero. The second occurs when the contributing trajectories undergo bifurcations. Close to the bifurcation the semiclassical formula diverges. More interestingly, in the example studied, *after* the bifurcation, where more than one trajectory satisfying the boundary conditions exist, only one of them in fact contributes to the semiclassical formula, a phenomenon closely related to Stokes lines. When the contributions of these trajectories are filtered out, the semiclassical results show excellent agreement with the exact calculations.

DOI: 10.1103/PhysRevE.69.066204 PACS number(s): 05.45.−a, 02.50.−r, 03.65.Sq, 31.15.Gy

I. INTRODUCTION

The coherent states of the harmonic oscillator provide a natural framework to study the semiclassical limit of quantum mechanics in phase space. They are perhaps what most closely resembles a classical particle, i.e., a localized Gaussian distribution of minimum uncertainty. The coherent state propagator $K(\mathbf{z}'',\mathbf{z}',T)=\langle \mathbf{z}''|e^{-i\hat{H}T/\hbar}|\mathbf{z}'\rangle$ represents the probability amplitude that the initial coherent state $|\mathbf{z}'\rangle$ evolves into another coherent state $|\mathbf{z}''\rangle$ after a time T. The semiclassical limit of the coherent state propagator was first considered by Klauder [1–3] and Weissman [4]. More recently, a detailed derivation of the semiclassical propagator for systems with one degree of freedom was presented in Ref. [5].

The semiclassical limit of $K(\mathbf{z}'',\mathbf{z}',T)$, similar to the semiclassical formulas for the propagator in the position or momentum representations, involves classical trajectories. The trajectories entering in $K(\mathbf{z}'',\mathbf{z}',T)$, however, are usually complex. Moreover, the Hamiltonian governing these trajectories is not the classical H, but a smoothed version $\tilde{H}\equiv\langle \mathbf{z}|\hat{H}|\mathbf{z}\rangle$. In fact, due to the overcomplete character of the coherent states basis, several different representations of the path integral exist [6], leading to different semiclassical limits [5]. One possible semiclassical approximation, for instance, involves yet a third Hamiltonian, different from both the classical H and the smoothed $\tilde{H}$, and which can be thought of as the antismoothed version of the classical Hamiltonian [5]. In this paper we shall consider only the more usual semiclassical formula, with $\tilde{H}$, which we discuss in Sec. III.

The first numerical evaluation of the semiclassical coherent state propagator was performed by Adachi [7] for the kicked rotator, a system whose dynamics is partly chaotic and partly regular. He emphasized that the semiclassical propagator, contrary to Klauder's expectations [3,8,9], is not free from the problem of caustics. Moreover, Adachi found solutions of the classical equations of motion, satisfying the necessary boundary conditions, that should *not* be taken into account in the semiclassical formula. These were called "noncontributing trajectories," and correspond to stationary points of the path integral whose steepest descent contour of integration cannot be deformed into the original contour of integration. The noncontributing points would be separated from the contributing ones by Stokes lines. A very interesting discussion of these topics was presented by Rubin and Klauder in Ref. [10] (see also Ref. [11]).

Other numerical investigations using the coherent state propagator were performed for a number of physically relevant systems with one degree of freedom, such as simple bound potentials [12,13], tunneling [14], and scattering systems [15]. More recently, systems with two degrees of freedom were also investigated [16,17]. The main difficulty that appears in all these applications is the calculation of complex classical trajectories. If $\tilde{H}$ is an analytic function of $\mathbf{q}$ and $\mathbf{p}$, the complexified dynamics can be mapped into that of a real Hamiltonian system with twice as many degrees of freedom [12,18,19]. The boundary conditions, however, are nontrivial, since they involve combinations of positions and momenta at the initial and final times. In this work we have used an adaptation of the method developed in Ref. [12] for Hamiltonians with one degree of freedom.

The purpose of this article is to present a numerical application of the semiclassical formula for the coherent state propagator for a soft-chaotic Hamiltonian system with two degrees of freedom. In this simplest time-independent situa-

tion where conservative chaos is possible, $K(\mathbf{z}'',\mathbf{z}',T)$ becomes a function of nine real variables: four "initial" and four "final" phase space coordinates plus the time T. In order to reduce the number of free variables, we shall restrict ourselves to the diagonal propagator $K(\mathbf{z},\mathbf{z},T)$. In this case we expect the real periodic trajectories to play an important role. We shall see that this is indeed the case. Furthermore, we choose to calculate $K(\mathbf{z},\mathbf{z},T)$ for $\mathbf{z}$ on a fixed energy shell, where $H(\mathbf{z},\mathbf{z}^*)=E$. Then, for each T, the number of variables is reduced to three, which turns out to be manageable.

We shall show that the semiclassical formula works generally very well throughout the phase space and for a wide range of times T. However, as remarked by Adachi [7], it is not free from caustics, nor from the problem of noncontributing classical trajectories. Eliminating these spurious contributions is not an easy task. Close to caustics, where bifurcations occur, the semiclassical formula diverges. After the bifurcation, where more than one trajectory exist, there are Stokes lines. One must identify these lines in order to decide which of the trajectories should be taken into account and which should be discarded. When the spurious trajectories are eliminated and one stays sufficiently far from the caustics, the semiclassical results are quite accurate. In particular, the fuzzy periodic orbits predicted in Sec. II, neatly seen in the exact (numerical) calculations, are faithfully reproduced by the semiclassical propagator. There are also other phase space structures in the exact propagator, not directly related to real periodic orbits. These turn out to be reproduced also in the semiclassical calculations, provided no attempt is made to approximate one step further and to express the results in terms of real periodic orbits instead of complex ones. This shows how important it is to carry out the semiclassical approximation in terms of complex classical orbits, and not to insist that these orbits somehow be made real.

We point out that our work differs from (and extends) that of Adachi in several respects. First of all we consider a full two degrees of freedom system, not a one-dimensional chaotic map. Moreover, for a given propagation time T and energy shell E (chosen to be almost completely chaotic) we place our coherent state $|\mathbf{z}\rangle$ at a grid of phase space points and propagate all of them, generating a complete picture of the propagator over the phase space. We also consider longer propagation times than those considered by Adachi, who restricts himself to short times only. As a result we find a larger number of noncontributing trajectories and are able to track the appearance of caustics as bifurcations of contributing ones.

The paper is organized as follows. In Sec. II we define the *return probability*, the main quantity to be calculated in the next sections. In Sec. III we present a brief derivation of the semiclassical coherent state propagator for systems with two degrees of freedom starting from path integrals. Section. IV is dedicated to the calculation of complex trajectories and in Sec. V we discuss the role of caustics as bifurcations of contributing trajectories. In Sec. VI we present numerical semiclassical results and compare them with numerical "exact" calculations. In order to understand the role of the noncontributing orbits and caustics, we show some of the "raw semiclassical data," including these two nonphysical contributions. After we filter them out, we compare the semiclassical plots with the exact calculations.

II. RETURN PROBABILITY AND PERIODIC ORBITS

The connection between classical mechanics and quantum mechanics can be examined in either direction. The usual way attempts to calculate quantal properties from classical data. This is called "quantization." It is the historical way since classical mechanics was well-established when quantum mechanics was being invented. Examples of quantization are the Gutzwiller trace formula [20] and the Bogomolny formula [21,22], yielding energy levels and wave functions in terms of classical periodic orbits. The hope of quantization is to produce exact quantal results, but this is very hard and it has not been achieved except in special cases. The opposite approach, sometimes referred to as "classicalization," starts from exact quantum data and uses them to calculate classical properties. It is free of the problems affecting quantization, such as nonconverging infinite sums. The only possible obstacle is the fact that some quantal behaviors have no classical equivalent. The present paper will contain examples of both quantization and classicalization. Let us begin with the latter.

Suppose that you have complete knowledge of quantum mechanics. Suppose that you use this knowledge to calculate the propagation of a wave packet, and that the packet is large enough at the start not to spread itself out of existence. Then, of course, the packet follows a classical trajectory approximately. And if, after time τ, you see the packet coming back to the place in phase space where it started, it must have been following a periodic orbit of period τ. Thus, if you can solve the quantum-mechanical problem, and if $\hbar$ is small enough, you can find the classical periodic orbits, or at least a fuzzy approximation to them, the fuzziness diminishing as $\hbar$ tends toward zero. This is an example of classicalization.

This idea was applied in Ref. [23] to the calculation of the quantal equivalent of the classical (E,τ) plot, which is the plot showing the connection between the energy and the period of families of periodic orbits. One of the things we shall do in the present work is to perform exact quantal calculations exhibiting the classical periodic orbits themselves, simultaneously with the relation between E and τ. To that effect, we shall calculate the return probability of a wave packet.

We consider a two-dimensional system with a time-independent Hamiltonian $\hat{H}$. Phase space is four-dimensional. We start at time 0 with a minimum-uncertainty Gaussian wave packet, or coherent state, $|\mathbf{z}\rangle \equiv |\mathbf{p},\mathbf{q}\rangle$ specified by its mean momentum $\mathbf{p}$ and its mean position $\mathbf{q}$. At time T the packet has evolved to $e^{-i\hat{H}T/\hbar}|\mathbf{p},\mathbf{q}\rangle$. The overlap of the evolved packet with the original one is

$$\Omega(\mathbf{p},\mathbf{q};T) = \langle \mathbf{p},\mathbf{q}|e^{-i\hat{H}T/\hbar}|\mathbf{p},\mathbf{q}\rangle. \tag{1}$$

This is large whenever the point $(\mathbf{p},\mathbf{q})$ is situated in phase space on or near a classical periodic orbit whose period τ is close to T.The absolute square of Ω

$$R(\mathbf{p},\mathbf{q};T) = |\Omega(\mathbf{p},\mathbf{q};T)|^2 \tag{2}$$

is the probability that the wave packet will return to its starting configuration after time T. By exploring R in phase

space, one gets a fuzzy picture of those periodic orbits whose τ is close to T.

The question is how best to represent this exploration of R, a function of five variables, in the two-dimensional publishing world. We like to think of the T dependence of R as a moving picture, although in this paper we shall only show "stills" from this movie. But there are four other variables p_x, p_y, q_x, q_y to contend with. We decided to fix the classical energy E of the packet. For motion in an ordinary potential $V(q_x, q_y)$, this is

$$E = (p_x^2 + p_y^2)/2 + V(q_x, q_y). \tag{3}$$

Fixing E is convenient for us because we calculate Ω, Eq. (1), by summing over the stationary states as intermediate states. The main contribution to this sum comes from quantal energies not too different from E, hence the sum is convergent. Given q_x, q_y, and E, the magnitude p of $\mathbf{p}$ is determined

$$p = \{2[E - V(q_x, q_y)]\}^{1/2} \tag{4}$$

and the only variable left is the direction θ of $\mathbf{p}$ such that $p_x = p \cos\theta$, $p_y = p \sin\theta$.

Thus, having fixed E and T, we want to look at the return probability as a function of the three variables q_x, q_y, θ

$$R(q_x, q_y, \theta; E, T). \tag{5}$$

Plotting a function of three variables is still a challenge. All our pictures of return probabilities were obtained by choosing a mesh in the $q_x q_y$ plane and then, at each point of this mesh, drawing a small polar plot (a "pawprint") representing R as a function of θ. The same units are used for R throughout the picture, of course. A big advantage of this kind of plot is that, at each $q_x q_y$, we get a visual sense, not only of the overall magnitude of R, but also of the direction in which the wavepacket must be launched to ensure a large return probability. In other words, the periodic orbits themselves jump out of the plot. In the following, both the exact quantal return probability (classicalization) and its semiclassical approximation (quantization) are plotted in this way.

III. THE SEMICLASSICAL PROPAGATOR IN TWO DIMENSIONS

The semiclassical limit of the coherent states propagator was derived in great detail in Ref. [5] for systems with one degree of freedom. In this section we derive the formula for two degrees of freedom. Since the main steps of the calculation are very similar to the one-dimensional case, we opted for a short presentation, referring to Ref. [5] for the details.

A. The coherent state propagator

For time-independent Hamiltonians, the coherent state propagator is defined by

$$K(\mathbf{z}''*, \mathbf{z}', T) = \langle \mathbf{z}'' | e^{-i\hat{H}T/\hbar} | \mathbf{z}' \rangle. \tag{6}$$

$|\mathbf{z}\rangle$ is the bidimensional coherent state of a harmonic oscillator of mass m and frequencies ω_x and ω_y,

$$|\mathbf{z}\rangle = e^{-(1/2)|\mathbf{z}|^2} e^{\mathbf{z}\cdot\hat{\mathbf{a}}^\dagger} |\mathbf{0}\rangle, \tag{7}$$

with $|\mathbf{0}\rangle$ the harmonic oscillator ground state and

$$\hat{a}_r^\dagger = \frac{1}{\sqrt{2}}\left(\frac{\hat{q}_r}{b_r} - i\frac{\hat{p}_r}{c_r}\right), \quad z_r = \frac{1}{\sqrt{2}}\left(\frac{q_r}{b_r} + i\frac{p_r}{c_r}\right). \tag{8}$$

$\hat{q}_r$, $\hat{p}_r$, and $\hat{a}_r^\dagger$ are the position, momentum, and creation operators, respectively; q_r and p_r are real numbers and z_r is complex. The index r assumes the values x and y and the dot in Eq. (7) stands for the scalar product. The parameters

$$b_r = (\hbar/m\omega_r)^{1/2} \text{ and } c_r = (\hbar m \omega_r)^{1/2} \tag{9}$$

define the length and momentum scales, respectively, and their product is $\hbar$. They are the coherent state widths along the coordinate and momentum axis, respectively. Finally, q_r and p_r are the average values of $\hat{q}_r$ and $\hat{p}_r$, respectively, and correspond to the center of the coherent state.

B. Path integral and stationary exponent approximation

The coherent states form an overcomplete set. This leads to a certain freedom in the construction of the path integral [5,6], allowing for many different representations of the propagator. Although all these representations are quantum mechanically equivalent, their semiclassical approximations may lead to different results [5], coinciding only in first order of $\hbar$. In this paper we shall adopt the most common representation, associated with the normal ordering of the operators $\hat{a}_r$ and $\hat{a}_r^\dagger$.

For bidimensional states, the unit operator is given by

$$1 = \int \frac{d^4\mathbf{z}}{\pi^2} |\mathbf{z}\rangle\langle\mathbf{z}| \equiv \int \frac{dq_x\, dq_y\, dp_x\, dp_y}{(2\pi\hbar)^2} |\mathbf{z}\rangle\langle\mathbf{z}|. \tag{10}$$

We divide the time T into N intervals of size ϵ and insert a unit operator between every two consecutive infinitesimal evolutions, so that Eq. (6) can be written as

$$K(\mathbf{z}''*, \mathbf{z}', T) = \int \prod_{j=1}^{N-1} \left(\frac{d^4\mathbf{z}_j}{\pi^2}\right) \times \prod_{k=0}^{N-1} \langle \mathbf{z}_{k+1} | e^{-i\hat{H}\epsilon/\hbar} | \mathbf{z}_k \rangle, \tag{11}$$

where we have identified $\mathbf{z}' \equiv \mathbf{z}_0$ and $\mathbf{z}'' \equiv \mathbf{z}_N$. The infinitesimal propagators $K_\epsilon(\mathbf{z}_{k+1}, \mathbf{z}_k, \epsilon) \equiv \langle \mathbf{z}_{k+1} | e^{-i\hat{H}\epsilon/\hbar} | \mathbf{z}_k \rangle$ can be calculated as usual by expanding the operator $e^{-i\hat{H}\epsilon/\hbar}$ to first order in ϵ and reexponentiating the result

$$\begin{aligned} \langle \mathbf{z}_{k+1} | e^{-i\hat{H}\epsilon/\hbar} | \mathbf{z}_k \rangle &\approx \langle \mathbf{z}_{k+1} | 1 - i\hat{H}\epsilon/\hbar | \mathbf{z}_k \rangle \\ &= \langle \mathbf{z}_{k+1} | \mathbf{z}_k \rangle \left(1 - iH_{k+1/2}\epsilon/\hbar\right) \\ &\approx \langle \mathbf{z}_{k+1} | \mathbf{z}_k \rangle e^{-iH_{k+1/2}\epsilon/\hbar}, \end{aligned} \tag{12}$$

where

$$\tilde{H}_{k+1/2} \equiv \frac{\langle \mathbf{z}_{k+1} | \hat{H} | \mathbf{z}_k \rangle}{\langle \mathbf{z}_{k+1} | \mathbf{z}_k \rangle}. \tag{13}$$

Using the overlap formula for coherent states

$$\langle \mathbf{z}|\mathbf{z}'\rangle = \exp\left[-\frac{|\mathbf{z}|^2}{2} - \frac{|\mathbf{z}'|^2}{2} + \mathbf{z}^* \cdot \mathbf{z}'\right], \tag{14}$$

we rewrite Eq. (11) as

$$K(\mathbf{z}''^*, \mathbf{z}', T) = \int \prod_{j=1}^{N-1} \left(\frac{d^4\mathbf{z}_j}{\pi^2}\right) e^{(i/\hbar)\mathcal{F}}, \tag{15}$$

where

$$e^{(i/\hbar)\mathcal{F}} \equiv \prod_{k=0}^{N-1} K_\epsilon(\mathbf{z}_{k+1}^*, \mathbf{z}_k, \epsilon) = \exp\left\{\sum_{k=0}^{N-1} \epsilon\left[-\frac{i}{\hbar}\tilde{H}_{k+1/2} + \frac{1}{2}\left(\frac{\mathbf{z}_{k+1}^* - \mathbf{z}_k^*}{\epsilon}\right)\cdot\mathbf{z}_k - \frac{1}{2}\left(\frac{\mathbf{z}_{k+1} - \mathbf{z}_k}{\epsilon}\right)\cdot\mathbf{z}_{k+1}^*\right]\right\}. \tag{16}$$

In the limit where $N\to\infty$ and $\epsilon\to 0$, with $N\epsilon = T$, Eq. (15) becomes a path integral representation of $K(\mathbf{z}'', \mathbf{z}', T)$. $\mathcal{F}$ plays the role of the action, as in the path integral in the position representation. However, as we shall see, it is not the actual action $\mathcal{S}$ which will appear later.

In the semiclassical limit $\hbar\to 0$, the main contributions to the integral come from the stationary points of $\mathcal{F}$. In the vicinity of each stationary point, $\mathcal{F}$ can be replaced by a quadratic form and the integrand can be replaced by a Gaussian. Since the integral (15) is $4(N-1)$ dimensional, so is each stationary point. Together they define a stationary trajectory in the four-dimensional phase space. The stationary exponent condition is

$$\delta\mathcal{F} = \sum_{j=1}^{N-1}\sum_{r=x}^{y}\left[\frac{\partial\mathcal{F}}{\partial z_{r,j}}\delta z_{r,j} + \frac{\partial\mathcal{F}}{\partial z_{r,j}^*}\delta z_{r,j}^*\right] = 0. \tag{17}$$

Considering independent variations of $\delta z_{r,j}$ and $\delta z_{r,j}^*$, we can write this condition explicitly as

$$-z_{r,k}^* + z_{r,k+1}^* = \frac{i\epsilon}{\hbar}\frac{\partial\tilde{H}_{k+1/2}}{\partial z_{r,k}},$$

$$z_{r,k} - z_{r,k+1} = \frac{i\epsilon}{\hbar}\frac{\partial\tilde{H}_{k+1/2}}{\partial z_{r,k+1}^*}, \tag{18}$$

where $k=1,\ldots,N-1$ in the first equation and $k=0,\ldots,N-2$ in the second equation.

C. Continuous variables and complexified phase space

In the limit $\epsilon\to 0$, Eqs. (18) become

$$\dot{z}_r = -\frac{i}{\hbar}\frac{\partial\tilde{H}}{\partial z_r^*} \quad\text{and}\quad \dot{z}_r^* = \frac{i}{\hbar}\frac{\partial\tilde{H}}{\partial z_r}, \tag{19}$$

where $\tilde{H}$, defined by Eq. (13), assumes the form $\tilde{H} = \langle \mathbf{z}|\hat{H}|\mathbf{z}\rangle$. The "smoothed Hamiltonian" $\tilde{H}(\mathbf{z}, \mathbf{z}^*)$ differs from the equivalent classical Hamiltonian $H(\mathbf{q}(\mathbf{z},\mathbf{z}^*), \mathbf{p}(\mathbf{z},\mathbf{z}^*))$ by terms of order $\hbar$. As discussed in Ref. [5] these differences are important and cannot be discarded.

In terms of the canonical variables q_r and p_r, Eqs. (19) are just Hamilton's equations for the Hamiltonian $\tilde{H}$. Since Eqs. (18) do not involve $z_{r,0}^*$ and $z_{r,N}$, the solutions of Eq. (19) that contribute to the semiclassical propagator must obey the boundary conditions $\mathbf{z}' = \mathbf{z}(0)$ and $\mathbf{z}''^* = \mathbf{z}^*(T)$; $\mathbf{z}^*(0)$ does not have to be equal to $\mathbf{z}'^*$ and $\mathbf{z}(T)$ does not have to be equal to $\mathbf{z}''$. These restrictions, which correspond to eight real constraints, make it generally impossible to find a solution of Eq. (19) in a four-dimensional real phase space. But solutions exist in a complexified phase space, where $\mathbf{z}^*$ is not the complex conjugate of $\mathbf{z}$. As we shall see in Sec. IV, this complex four-dimensional phase space can be mapped into a real eight-dimensional phase space governed by the real part of $\tilde{H}$.

To avoid confusion with complex numbers and their complex conjugates, we rename the variables $\mathbf{z}\to\mathbf{u}$ and $\mathbf{z}^*\to\mathbf{v}$:

$$z_r \to u_r = \frac{1}{\sqrt{2}}\left(\frac{q_r}{b_r} + i\frac{p_r}{c_r}\right),$$

$$z_r^* \to v_r = \frac{1}{\sqrt{2}}\left(\frac{q_r}{b_r} - i\frac{p_r}{c_r}\right). \tag{20}$$

q_r and p_r are now complex variables and $\mathbf{u}\neq\mathbf{v}^*$ in general. In this notation Hamilton's equations (19) read

$$i\hbar\dot{u}_r = \frac{\partial\tilde{H}}{\partial v_r} \quad\text{and}\quad -i\hbar\dot{v}_r = \frac{\partial\tilde{H}}{\partial u_r}, \tag{21}$$

with boundary conditions

$$u_r' \equiv u_r(0) = z_r' = \frac{1}{\sqrt{2}}\left(\frac{q_r'}{b_r} + i\frac{p_r'}{c_r}\right),$$

$$v_r'' \equiv v_r(T) = z_r''^* = \frac{1}{\sqrt{2}}\left(\frac{q_r''}{b_r} - i\frac{p_r''}{c_r}\right). \tag{22}$$

We emphasize that q_r', p_r', q_r'', and p_r'', the labels of the coherent states $|\mathbf{z}'\rangle$ and $|\mathbf{z}''\rangle$, are real parameters. The variables $\mathbf{u}''\equiv\mathbf{u}(T)$ and $\mathbf{v}'\equiv\mathbf{v}(0)$ are not restricted by the boundary conditions. They are determined by the integration of Hamilton's equations (21).

When $\mathcal{F}$ is calculated at the stationary trajectory and the limit $\epsilon\to 0$ is taken, the sum over k in Eq. (16) becomes an integral over the trajectory from $t=0$ to $t=T$. The value of $\mathbf{u}(T)$ as computed from the continuous trajectory is, as we just discussed, different from $\mathbf{z}''$. Similarly, the value taken by $\mathbf{v}(0)$ is generally different from $\mathbf{z}'^*$. But in expression (16), $\mathbf{u}_N$ or $\mathbf{z}_N$ was $\mathbf{z}''$ and $\mathbf{v}_0$ or $\mathbf{z}_0^*$ was $\mathbf{z}'^*$. Therefore, if we just replaced $\mathbf{z}_0^*$ by $\mathbf{v}_0$ and $\mathbf{z}_N$ by $\mathbf{u}_N$, we would make a mistake. To correct this mistake, we must take out from the sum the two terms containing $\mathbf{u}_N$ and $\mathbf{v}_0$, namely, $-\frac{1}{2}\mathbf{v}_N\cdot\mathbf{u}_N$ and $-\frac{1}{2}\mathbf{v}_0\cdot\mathbf{u}_0$, and replace them by their correct values, namely, $-\frac{1}{2}|\mathbf{z}''|^2$ and $-\frac{1}{2}|\mathbf{z}'|^2$. Consequently, the value of $\mathcal{F}$ in the limit $\epsilon\to 0$ becomes [5]

$$\frac{i}{\hbar}\mathcal{F}=\int_0^T\left[\tfrac{1}{2}(\dot{\mathbf{v}}\cdot\mathbf{u}-\mathbf{v}\cdot\dot{\mathbf{u}})-\frac{i}{\hbar}\tilde{H}(\mathbf{u},\mathbf{v})\right]dt + \tfrac{1}{2}(\mathbf{u}'\cdot\mathbf{v}'+\mathbf{u}''\cdot\mathbf{v}'')-\tfrac{1}{2}(|\mathbf{z}'|^2+|\mathbf{z}''*|^2). \quad (23)$$

The complex action is defined as the first two terms of Eq. (23),

$$\frac{i}{\hbar}\mathcal{S}(\mathbf{v}'',\mathbf{u}',T)=\int_0^T\left[\frac{1}{2}(\dot{\mathbf{v}}\cdot\mathbf{u}-\mathbf{v}\cdot\dot{\mathbf{u}})-\frac{i}{\hbar}\tilde{H}(\mathbf{u},\mathbf{v})\right]dt + \frac{1}{2}(\mathbf{u}'\cdot\mathbf{v}'+\mathbf{u}''\cdot\mathbf{v}''). \quad (24)$$

This quantity has properties similar to the usual action of real Hamiltonian systems, namely,

$$\frac{\partial\mathcal{S}}{\partial v_r''}=-i\hbar u_r'', \quad \frac{\partial\mathcal{S}}{\partial u_r'}=-i\hbar v_r', \quad \frac{\partial\mathcal{S}}{\partial T}=-\mathcal{E}, \quad (25)$$

where $\mathcal{E}=\tilde{H}(\mathbf{u}',\mathbf{v}')=\tilde{H}(\mathbf{u}'',\mathbf{v}'')$ is the complex energy.

D. The Gaussian integral

Once the stationary trajectory has been found, the integrals in Eq. (15) can be calculated in the Gaussian approximation. Expanding $\mathcal{F}$ up to second order around the stationary trajectory $\mathcal{F}\approx\mathcal{F}_0+1/2\delta^2\mathcal{F}$, we obtain

$$K(\mathbf{z}''*,\mathbf{z}',T)=e^{(i/\hbar)\mathcal{F}_0}\int\prod_{j=1}^{N-1}\left(\frac{d^4\mathbf{z}_{(j)}}{\pi^2}\right)e^{(i/2\hbar)\delta^2\mathcal{F}}, \quad (26)$$

where $\mathcal{F}_0$ is the phase $\mathcal{F}$ calculated at the stationary trajectory. This integral was calculated in great detail in Ref. [5] for systems with one degree of freedom. For the present case of two spatial dimensions, the calculation is similar, but more involved. Here we shall simply write down the result, leaving the details of the calculation for a future publication [24]. We find

$$\int\prod_{j=1}^{N-1}\left(\frac{d^4\mathbf{z}_j}{\pi^2}\right)e^{(i/2\hbar)\delta^2\mathcal{F}}=\frac{e^{[-(i/2)\sigma+(i/\hbar)\mathcal{I}]}}{\sqrt{|\det(M_{\mathbf{vv}})|}}, \quad (27)$$

where $M_{\mathbf{v}\,\mathbf{v}}$ is a 2×2 block of the complex tangent matrix M, defined by

$$\begin{pmatrix}\delta\mathbf{u}''\\ \delta\mathbf{v}''\end{pmatrix}=\underbrace{\begin{pmatrix}M_{\mathbf{uu}} & M_{\mathbf{uv}}\\ M_{\mathbf{vu}} & M_{\mathbf{vv}}\end{pmatrix}}_{M}\begin{pmatrix}\delta\mathbf{u}'\\ \delta\mathbf{v}'\end{pmatrix}, \quad (28)$$

where $\delta\mathbf{u}'$, $\delta\mathbf{v}'$ are small displacements around the stationary trajectory at $t=0$ and $\delta\mathbf{u}''$, $\delta\mathbf{v}''$ are the propagated displacements at $t=T$. The quantity $\mathcal{I}$ is

$$\mathcal{I}=\frac{1}{2}\int_0^T\left(\frac{\partial^2\tilde{H}}{\partial u_x\partial v_x}+\frac{\partial^2\tilde{H}}{\partial u_y\partial v_y}\right)dt \quad (29)$$

and σ is the phase of $\det(M_{\mathbf{v}\,\mathbf{v}})$.

E. The semiclassical propagator

Putting Eqs. (26), (23), (24), and (27) together we obtain the final expression for the semiclassical propagator:

$$K(\mathbf{z}''*,\mathbf{z}',T)\simeq\sum_{\text{traj}}\frac{e^{-(i/2)\sigma}}{\sqrt{|\det M_{\mathbf{vv}}|}}\times\exp\left[\frac{i}{\hbar}(\mathcal{S}+\mathcal{I})-\frac{1}{2}(|\mathbf{z}'|^2+|\mathbf{z}''|^2)\right]. \quad (30)$$

The sum indicates that, in principle, all stationary trajectories satisfying the boundary conditions (22) should be included (see, however, the discussion in Sec. VI about noncontributing trajectories).

The propagator has nine real parameters: four initial labels q_x',q_y',p_x',p_y', four final labels q_x'',q_y'',p_x'',p_y'', and the time T. In this paper, we shall restrict ourselves to the diagonal propagator, $\mathbf{z}''=\mathbf{z}'\equiv\mathbf{z}$, reducing the number of independent parameters to 5. In this case, if a stationary trajectory happens to be real, then it is also periodic and M is its monodromy matrix. For generic values of $\mathbf{z}$ and T, however, the stationary trajectories are complex and nonperiodic. The Fourier transform of the diagonal propagator is the diagonal Green's function $G(\mathbf{z},E)$. For bound systems it has poles at the energy levels E_n and the residues are the Husimi functions $|\langle\mathbf{z}|\Psi_n\rangle|^2$. The semiclassical limit of $G(\mathbf{z},E)$ will be considered in Ref. [24].

From the classical mechanics point of view, the transition probability from the point $\mathbf{z}'$ to $\mathbf{z}''$ is 1 if there is a real trajectory connecting the initial and the final points in time T, and 0 otherwise. In the semiclassical limit we expect large contributions to the propagator if $\mathbf{z}''$ happens to be on the real trajectory through $\mathbf{z}'$, separated by a time interval T. Otherwise the trajectory satisfying Eqs. (21) and (22) is complex and the more it wanders into the complex plane, the less it should contribute to the propagator. Therefore, according to Eq. (30), we expect the total exponent

$$F\equiv\mathcal{S}+\mathcal{I}+\frac{i\hbar}{2}(|\mathbf{z}'|^2+|\mathbf{z}''|^2)-\frac{\hbar\sigma}{2} \quad (31)$$

to have a *positive* imaginary part for complex trajectories. As we shall see in Sec. VI, this is almost always the case. There are, however, exceptions, that we shall discuss momentarily. Note that σ is always real (and therefore does not contribute to the imaginary part of F) and that $|\mathbf{z}'|^2$ and $|\mathbf{z}''|^2$ are of the order of $\hbar^{-1}$ [see Eqs. (7) and (8)].

Equation (30) involves four classical quantities: $\mathcal{S}$, $M_{\mathbf{vv}}$, σ, and $\mathcal{I}$. The role of $\mathcal{I}$ was discussed in Ref. [5]. It is a kind of compensation for the appearance of the smoothed dynamics $\tilde{H}$ instead of the classical H. For a harmonic oscillator, $\mathcal{S}+\mathcal{I}$ is identical to the action computed with the classical H. For nonharmonic Hamiltonians, the compensation is only approximate.

The prefactor $|\det M_{\mathbf{vv}}|^{-1/2}$, also plays a very important role in the semiclassical formula. It contains information about the neighborhood of the stationary trajectory. Unstable trajectories, for example, are expected to contribute less than

stable ones. Finally, σ controls the relative phase of the different trajectories contributing to the propagator.

IV. THE CALCULATION OF COMPLEX TRAJECTORIES

If $\widetilde{H}$ is an analytic function of q_x, q_y, p_x, and p_y, the four-dimensional complex phase space can be mapped into an eight-dimensional real phase space, where the usual methods of Hamiltonian dynamics can be applied [12,18,19]. Therefore, assuming $\widetilde{H}$ to be analytic we define real variables x_i and p_i by

$$q_x = x_1 + ix_3, \quad p_x = p_1 - ip_3,$$

$$q_y = x_2 + ix_4, \quad p_y = p_2 - ip_4. \tag{32}$$

By the Cauchy-Riemman conditions, Hamilton's Eqs. (21) become

$$\dot{x}_j = \frac{\partial \,\mathrm{Re}(\widetilde{H})}{\partial p_j} \text{ and } \dot{p}_j = -\frac{\partial \,\mathrm{Re}(\widetilde{H})}{\partial x_j}, \tag{33}$$

where $\mathrm{Re}[\widetilde{H}]$ is the real part of $\widetilde{H}$ and $j=1$, 2, 3, and 4. The boundary conditions (22) for the diagonal propagator become

$$q_x = x_1(0) + \frac{b_x}{c_x}p_3(0) = x_1(T) - \frac{b_x}{c_x}p_3(T),$$

$$p_x = p_1(0) + \frac{c_x}{b_x}x_3(0) = p_1(T) - \frac{c_x}{b_x}x_3(T),$$

$$q_y = x_2(0) + \frac{b_y}{c_y}p_4(0) = x_2(T) - \frac{b_y}{c_y}p_4(T),$$

$$p_y = p_2(0) + \frac{c_y}{b_y}x_4(0) = p_2(T) - \frac{c_y}{b_y}x_4(T). \tag{34}$$

The search for complex trajectories in a four-dimensional phase space is then reduced to that of real trajectories in eight-dimensions satisfying the eight mixed boundary conditions above. We have used an adaptation of the numerical method developed in Ref. [12] (which, in turn, is an adaptation of the monodromy method for periodic orbits [25]) to find the trajectories for given q_x, q_y, p_x, p_y, and T.

V. BIFURCATIONS AND FOCAL POINTS

The semiclassical propagator, Eq. (30), diverges when $|\det M_{\mathbf{vv}}| \to 0$. In this section we show that this happens whenever a bifurcation occurs. These are bifurcations of complex, nonperiodic trajectories, and they take place as follows: the semiclassical propagator $K(\mathbf{z}''^*, \mathbf{z}', T)$ depends on the classical trajectory satisfying $\mathbf{u}(0)=\mathbf{z}'$ and $\mathbf{v}(T)=\mathbf{z}''^*$. The set of classical solutions satisfying these boundary conditions form one parameter families as a function of T. If T is small, there is usually a single solution of Hamilton's equations satisfying the boundary conditions. As T increases, however, the family might branch into two or more, producing the bifurcation. Close to the bifurcation point there are two (or more) nearby trajectories, differing by small displacements $\delta\mathbf{u}(t) \neq 0$ and $\delta\mathbf{v}(t) \neq 0$, and satisfying $\delta\mathbf{u}' = \delta\mathbf{v}'' = 0$. At the bifurcation point, there must exist nontrivial solutions of the equation [see Eq. (28)]

$$\begin{pmatrix} \delta\mathbf{u}'' \\ 0 \end{pmatrix} = \begin{pmatrix} M_{\mathbf{uu}} & M_{\mathbf{uv}} \\ M_{\mathbf{vu}} & M_{\mathbf{vv}} \end{pmatrix} \begin{pmatrix} 0 \\ \delta\mathbf{v}' \end{pmatrix}, \tag{35}$$

implying that $\det[M_{\mathbf{vv}}]=0$ and leading to the divergence of the semiclassical formula (30). The eigenvector corresponding to the null eigenvalue of $M_{\mathbf{vv}}$ indicates the initial condition of the bifurcated trajectory.

These bifurcations imply the existence of focal points in the complex phase space. To see this we write the tangent matrix M in terms of second derivatives of the complex action (24). From Eqs. (25) we have

$$-i\hbar\,\delta v_r' = \delta\left(\frac{\partial \mathcal{S}}{\partial u_r'}\right) \text{ and } -i\hbar\,\delta u_r'' = \delta\left(\frac{\partial \mathcal{S}}{\partial v_r''}\right). \tag{36}$$

Computing the variation on the right-hand sides and rearranging the terms so as to write $\delta\mathbf{u}''$ and $\delta\mathbf{v}''$ as functions of $\delta\mathbf{u}'$ and $\delta\mathbf{v}'$ we get [see Eq. (28)]

$$\frac{i}{\hbar}M_{\mathbf{vv}} = \left(\frac{\partial^2 S}{\partial \mathbf{v}'' \partial \mathbf{u}'}\right)^{-1} = \begin{pmatrix} \dfrac{\partial^2 \mathcal{S}}{\partial v_x'' \partial u_x'} & \dfrac{\partial^2 \mathcal{S}}{\partial v_y'' \partial u_x'} \\ \dfrac{\partial^2 \mathcal{S}}{\partial v_x'' \partial u_y'} & \dfrac{\partial^2 \mathcal{S}}{\partial v_y'' \partial u_y'} \end{pmatrix}^{-1}. \tag{37}$$

Using Eqs. (25) again we obtain

$$M_{\mathbf{vv}} = \left(\frac{\partial v_x'}{\partial v_x''}\frac{\partial v_y'}{\partial v_y''} - \frac{\partial v_y'}{\partial v_x''}\frac{\partial v_x'}{\partial v_y''}\right)^{-1} \begin{pmatrix} \dfrac{\partial v_y'}{\partial v_y''} & -\dfrac{\partial v_x'}{\partial v_y''} \\ -\dfrac{\partial v_y'}{\partial v_x''} & \dfrac{\partial v_x'}{\partial v_x''} \end{pmatrix}. \tag{38}$$

Thus, the prefactor can be written as

$$|\det M_{\mathbf{vv}}|^{-1/2} = \left| \frac{\partial v_x'}{\partial v_x''}\frac{\partial v_y'}{\partial v_y''} - \frac{\partial v_y'}{\partial v_x''}\frac{\partial v_x'}{\partial v_y''} \right|^{1/2}. \tag{39}$$

For one-dimensional systems this reduces to $|\partial v'/\partial v''|^{1/2}$. It diverges when a small displacement $\delta v'$ at $t=0$ leads to the same end point v'' at time T, implying $\delta v''=0$ and characterizing a focal point, or caustic. In two dimensions the prefactor is more complicated and the focal point can occur generally in four different ways. As an example, it occurs when a small displacement in the x direction $\delta v_x'$ at $t=0$ leads to the same end point in the y direction v_y'' at time T. In general it occurs when a particular combination of $\delta v_x'$ and $\delta v_y'$, corresponding to the null eigenvector of $M_{\mathbf{vv}}$, leads to $\delta\mathbf{v}''=0$.

In any case, we expect the semiclassical approximation to fail near such bifurcations. We shall see examples of them in Sec. VI.

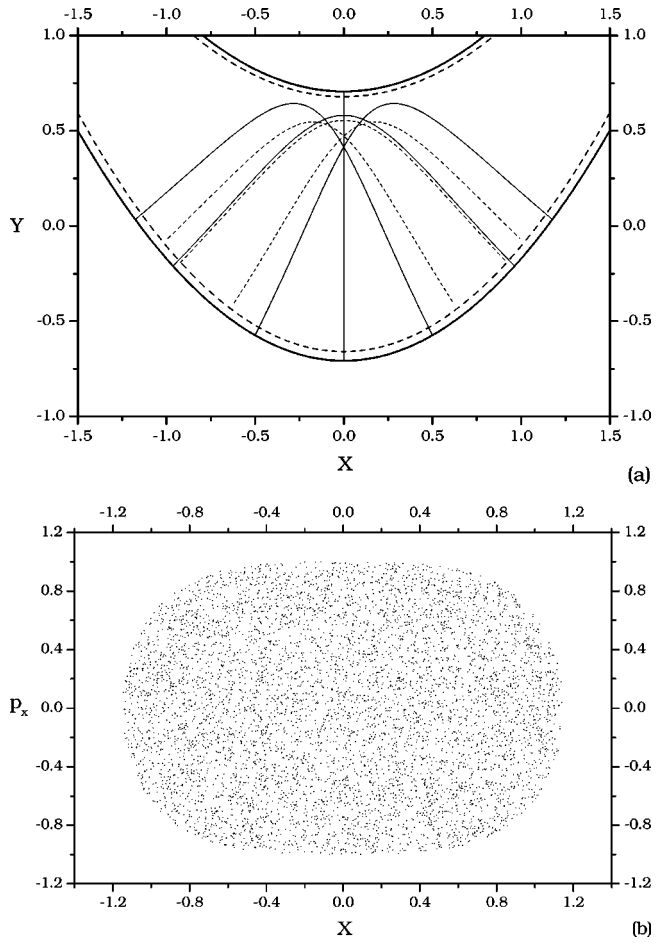

FIG. 1. Shortest periodic trajectories (a) and (x,p_x) Poincaré section (b) at $E=0.5$. The dotted lines show the periodic orbits of smoothed Hamiltonian $\tilde{H}$ and the full lines show the corresponding periodic orbits of the classical Hamiltonian H. The approximate periods of the orbits are 4.44 for the vertical oscillation, 7.1 for the boomerang shaped symmetric orbit, and 7.4 for the pair of asymmetric orbits. The equipotential lines at $V=0.5$ (solid) and $\tilde{V}=0.5$ (dotted) are also displayed.

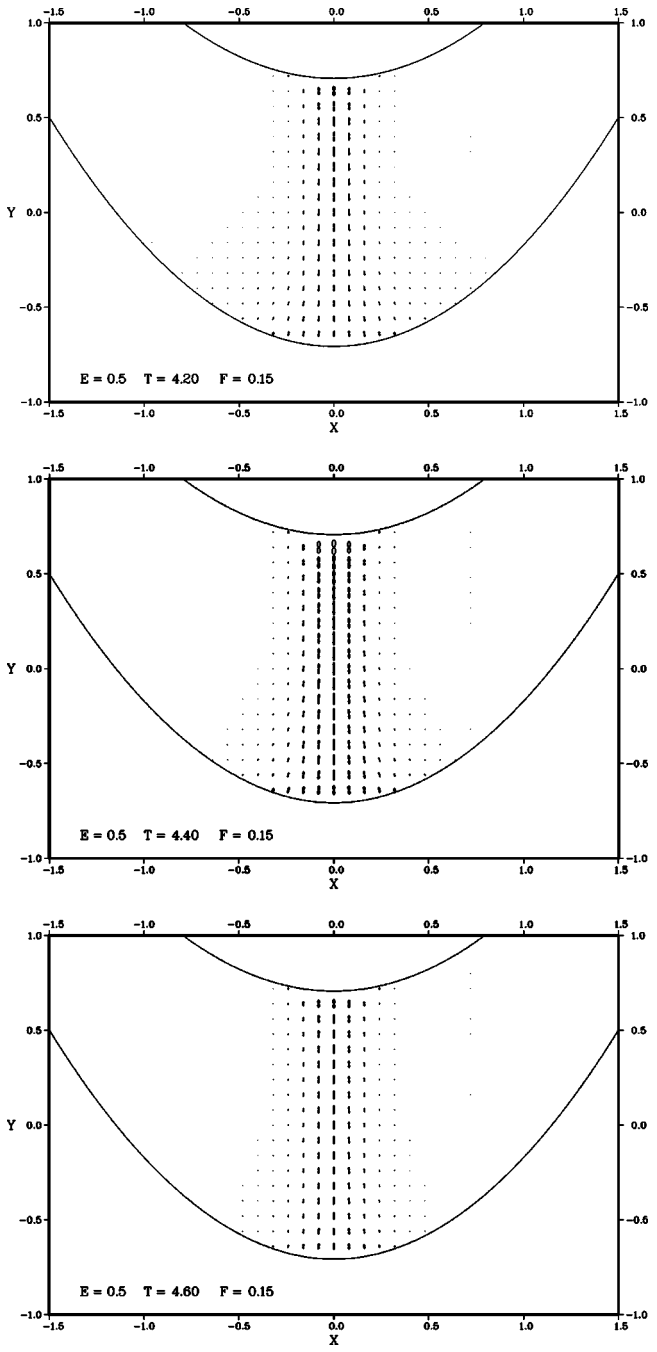

FIG. 2. Exact return probability for propagation times $T=4.2$, 4.4, and 4.6. The period of the vertical periodic orbit is $T\approx 4.44$.

VI. A NUMERICAL EXAMPLE: THE RETURN PROBABILITY

A. The Nelson Hamiltonian

As an application of the semiclassical theory developed in the previous sections, we compute the return probability, as defined by Eqs. (1)–(5) of Sec. II, for a Hamiltonian system with two degrees of freedom. We shall present numerical comparisons between the exact return probability, computed directly from the eigenfunctions of the Hamiltonian, and the semiclassical return probability, computed from complex trajectories. We have chosen the Nelson potential, given by

$$V(x,y) = (y - x^2/2)^2 + 0.05x^2$$

for our numerical study. In this section we shall use x and y instead of q_x and q_y. This system has been widely investigated, both classically [25–27] and quantum mechanically [22,23,28,29]. In the present calculations we have chosen to work on the energy surface $E=0.5$, which corresponds to a mostly chaotic region of phase space, in the sense that the shortest periodic orbits are all unstable. Nonetheless, the Lyapunov exponent of the shortest orbit times its period is about 2.06. We also have chosen $\hbar=0.05$ and, for the widths of the initial wave packets $b_x=b_y=b=0.2$, which implies $c_x=c_y=c=\hbar/b=0.25$.

We computed $R(x,y,\theta;E=0.5,T)$ from $T=0$ to $T=9$ in steps of 0.1. Figure 1(a) displays all the periodic orbits in this range of T for energy 0.5. The shortest periodic orbit is a harmonic oscillation along the y axis, called the "vertical orbit," with $T\approx 4.44$. The next shortest orbit is a symmetric

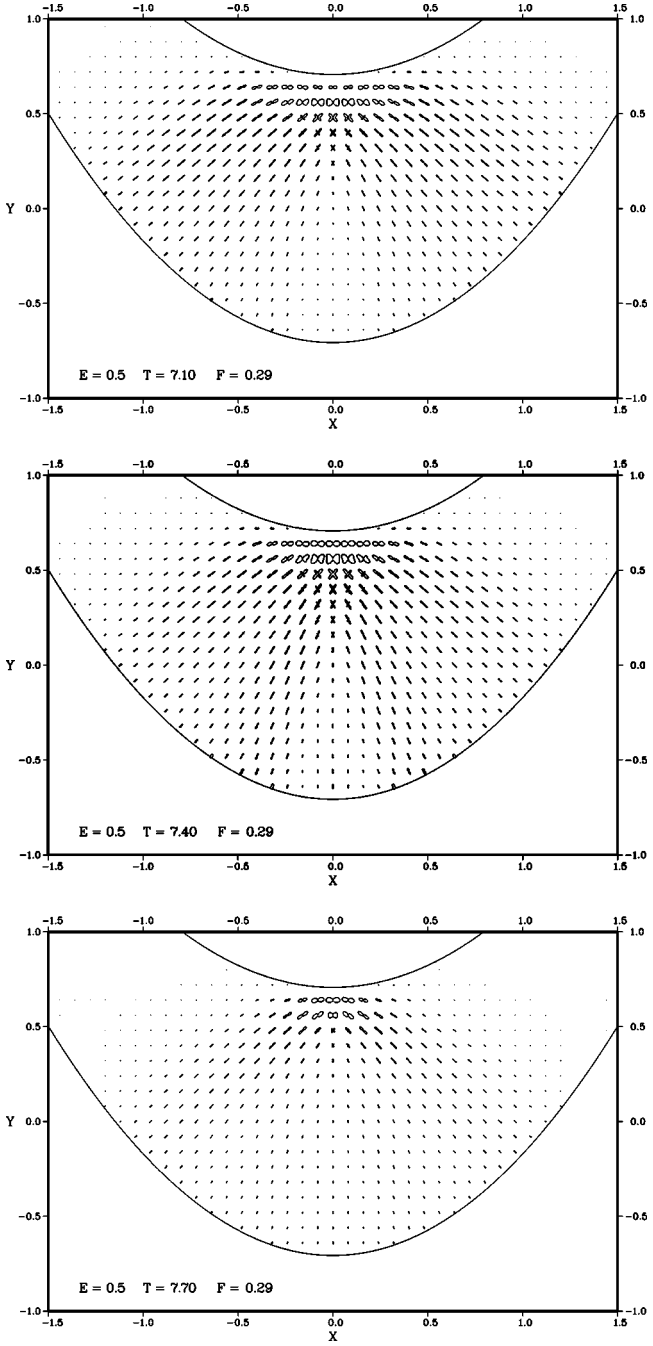

FIG. 3. Exact return probability for propagation times $T=7.1$, 7.4, and 7.7.

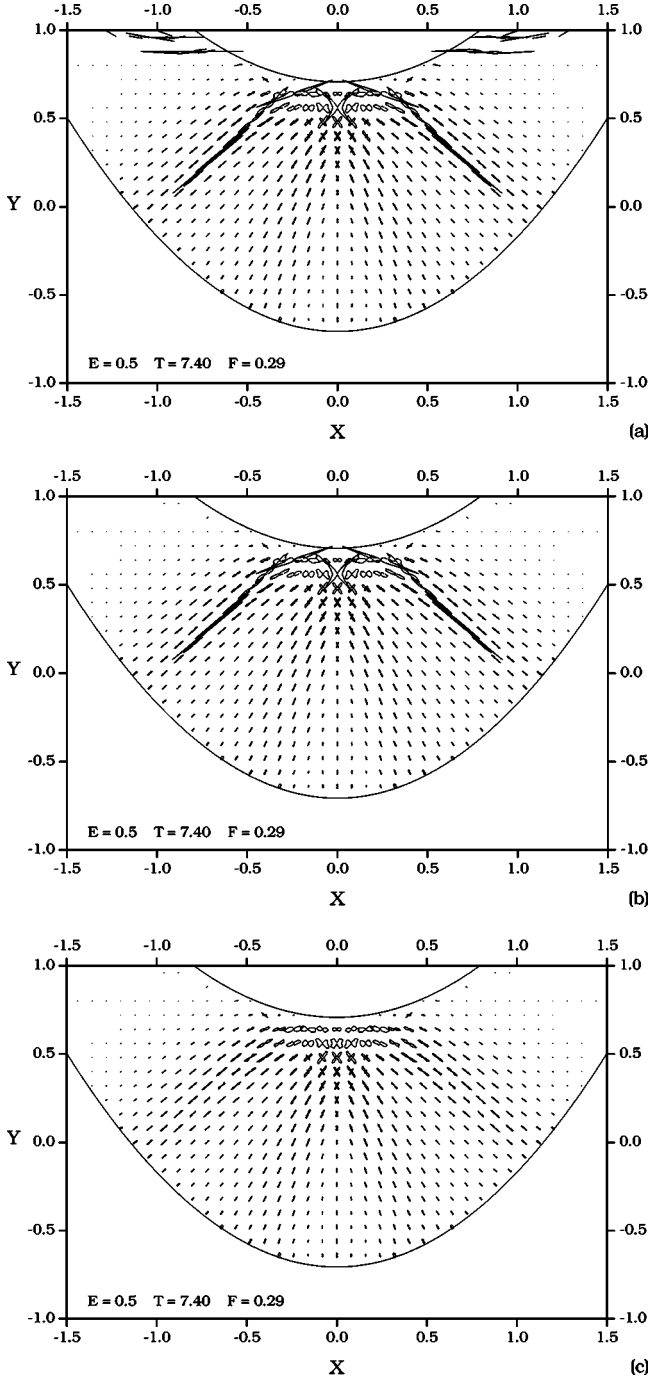

FIG. 4. Semiclassical return probability for $T=7.4$: (a) including the contributions of all complex trajectories, except those whose individual contribution gives $R>1$, (b) all trajectories with $\mathrm{Im}\,F<0$ have been removed, (c) all $x-y-\theta$ points close to caustics have been removed.

libration with $T\approx 7.1$, followed by a pair of symmetry-related asymmetric librations with $T\approx 7.4$. Finally, there is the first repetition of the vertical orbit at $T\approx 8.88$. The full lines show the periodic orbits of the classical Hamiltonian H, whereas the dotted lines show the corresponding periodic orbits of the smoothed Hamiltonian $\tilde{H}$. The equipotential lines at $V(x,y)=0.5$ and $\tilde{V}\equiv\langle \mathbf{z}|V(\hat{x},\hat{y})|\mathbf{z}\rangle=0.5$ are also displayed. Figure 1(b) shows the (x,p_x) Poincaré section of $\tilde{H}$ at the same energy. There is no qualitative difference between the Poincaré sections of $\tilde{H}$ and H at this energy.

B. Exact results

We display the return probability, both exact and semiclassical, in (x,y,θ) pawprint plots, or minipolar plots, as explained at the end of Sec. II. For the figures below we have used equally spaced x,y points at intervals of 0.08 in both directions. For each x and y on the mesh, we make a second mesh, this time over θ, from 0° to 360° in steps of 10°. Thus,

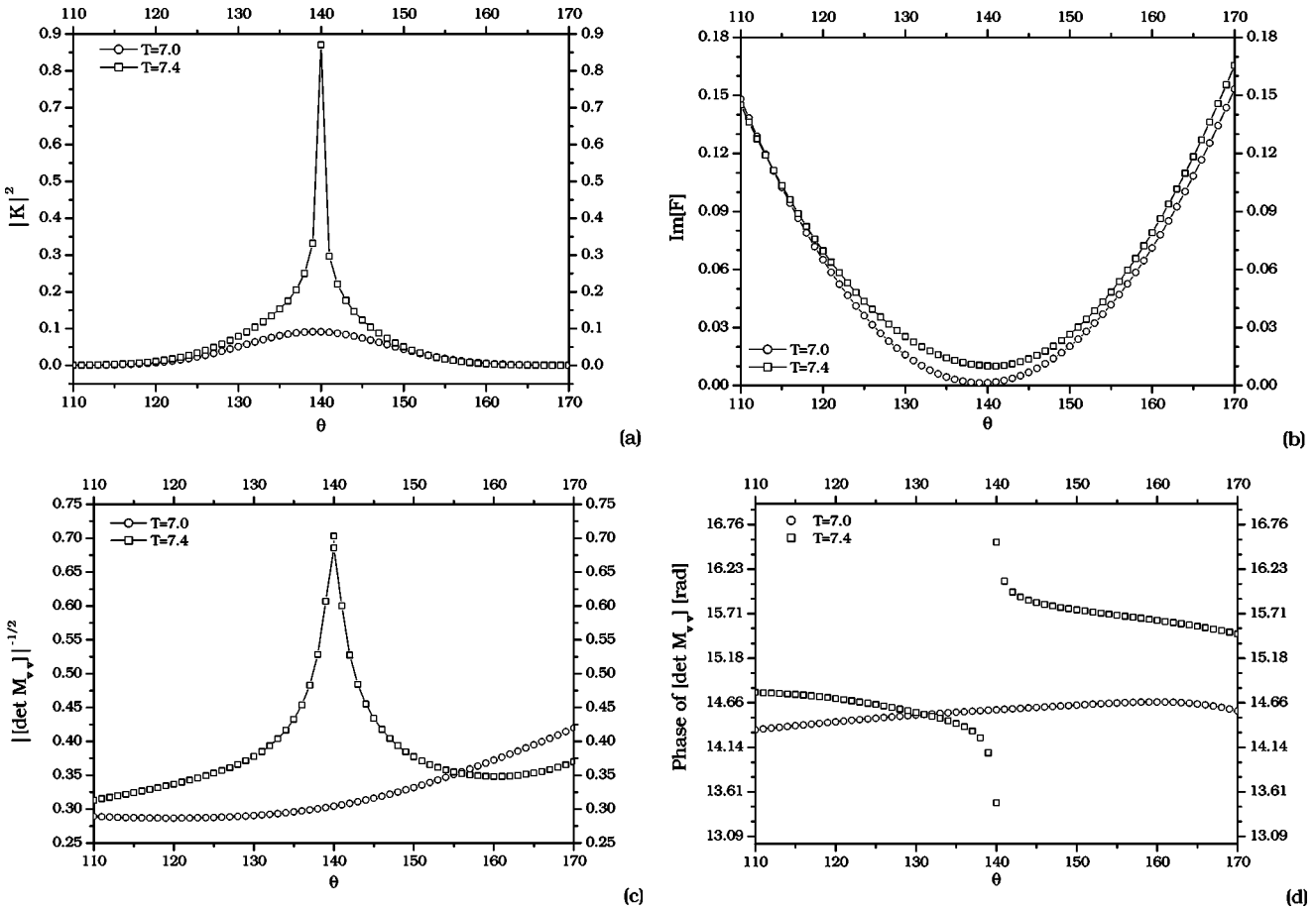

FIG. 5. Comparison between the return probabilities for $x=0.72$, $y=0.24$, and $E=0.5$ as a function of θ (in degrees) for $T=7.0$ (circles) and $T=7.4$ (squares). (a) Return probability, (b) imaginary part of the total exponent F; (c) prefactor $|\det(M_{\mathbf{vv}})|^{-1/2}$, (d) phase σ of prefactor. Panels (c) and (d) show that there are two orbits contributing at $\theta=140$ with σ differing by π.

centered at each x,y point, we draw the pawprint, a tiny polar plot of 36 points with equally spaced θ's, each radius being proportional to $R(x,y,\theta)$ (we are omitting the labels E and T). We connect the 36 points with straight lines. Since the value of $R(x,y,\theta)$ could sometimes be too large or too small, we have multiplied $R(x,y,\theta)$ by a constant factor F, which is shown on the figures, so as to make the pawprints visible but separate. This way of plotting R is very effective, since it shows both the intensity of the contributing classical trajectory and the direction in which it is going.

Figure 2 shows three sets of mini polar plots for T close to the period of the shortest periodic orbit: $T=4.2$, $T=4.4$, and $T=4.6$. The plots show the fuzzy quantal image of the classical vertical trajectory forming near the y axis as T approaches the orbit's period, 4.44. If one tried to make a similar plot for a value of T far from the period of the periodic trajectory, such as $T=3$ or $T=5.5$, one would see nothing, because R for such a T would be extremely small at all points and all angles. As T gets close to 7.1, a new structure emerges, and the quantum image of the symmetric libration becomes clear. This is shown in Fig. 3, which displays polar plots of the return probability for three values of T: 7.1, 7.4, and 7.7. For T close to 7.4 the asymmetric libration becomes subtly visible. When T nears 7.7, both of these orbits go away and a different pattern takes over: an upside down "V" shape. This structure, although "neat," does not correspond to a real periodic orbit of the Nelson Hamiltonian. We shall return to it.

C. Noncontributing trajectories and bifurcations

The semiclassical construction of one of our plots requires the calculation of at least 36 complex trajectories for each x,y point on the mesh. Finding these complex solutions is no easy task. Our search algorithm, based on Newton's method, uses nearby real periodic orbits as starting points. For systems with two or more degrees of freedom there may be more than one such nearby orbit [see Fig. 1(a)]. Therefore, for some values of x, y, and θ, the method may find (converge to) more than one trajectory satisfying the appropriate boundary conditions. Such a trajectory may be buried deep in the complex phase space. If the imaginary part of the total exponent F is large and positive, the contribution to the propagator is negligible. Including this trajectory or not makes essentially no difference. There are, however, other situations where more than one trajectory exist and where careful analysis is needed to decide whether or not to include them in the semiclassical formula. In this subsection we consider these cases in detail.

Figure 4(a) shows an example of a semiclassical plot, for $T=7.4$, where the contributions of almost all trajectories

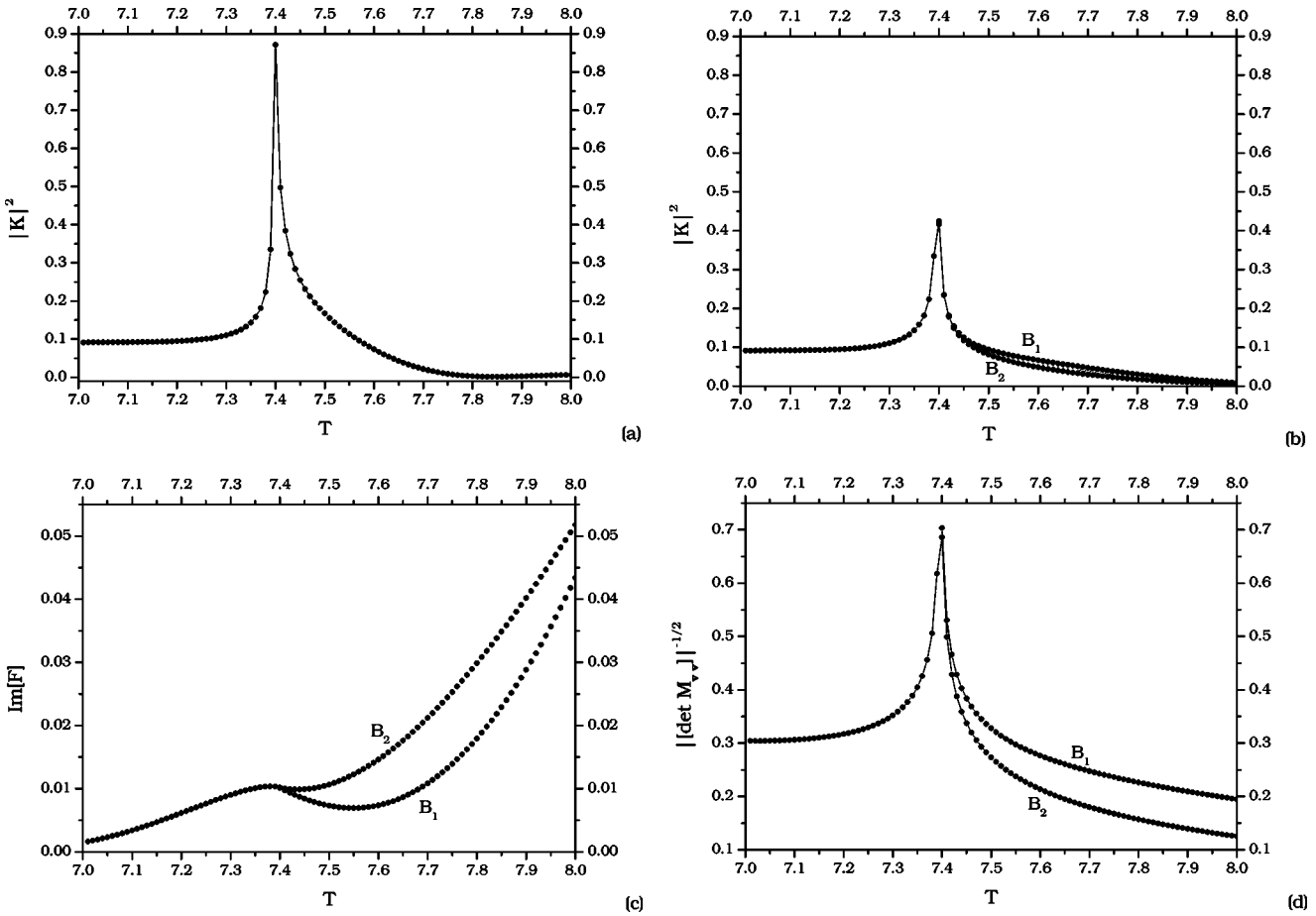

FIG. 6. Bifurcation of the trajectory for $x=0.72$, $y=0.24$, $E=0.5$, and $\theta=140$ as a function of T: (a) return probability with all contributions added. Panels (b)–(d) show the individual contribution of each trajectory separately: (b) return probability, (c) imaginary part of F, (d) prefactor. The branches after the bifurcation are labeled B_1 and B_2.

found by our search method were taken into account. The only trajectories removed were those which, alone, would make R larger than 1. Even after these trajectories have been removed, several large contributions, not present in the corresponding exact plot, can still be seen. Many of the trajectories responsible for these large contributions, have a negative imaginary part of F. This type of trajectory does not exist for the one-dimensional harmonic oscillator, where $\mathrm{Im}(F)=\hbar|z|^2(1+\cos\omega T)$ is always non-negative. But they do exist in other, nonlinear, one-dimensional problems [12,13]. As discussed in Refs. [7,13], these trajectories are probably related to forbidden deformations of the integration contour in the stationary phase approximation, and should not be included in the semiclassical calculation. Including them would result in exponentially large contributions to the propagator as $\hbar$ goes to zero [see Eqs. (30) and (31) and Ref. [10]]. These trajectories are easy to identify and remove.

In Fig. 4(b) all trajectories with $\mathrm{Im}(F)<0$ have been removed. It is clear that several other spurious contributions remain. Most of these large values attained by the return probability have to do with bifurcations, or focal points (or caustics), which separate regions where different number of trajectories contribute to the propagator. As discussed in Sec. V, the semiclassical propagator diverges at focal points, and is not a good approximation in their neighborhood.

Figure 5 shows a comparison between the semiclassical return probabilities at the point $x=0.72$, $y=0.24$, and $E=0.5$, as a function of θ, for two times $T=7.0$ and $T=7.4$. The latter is one of the points in Fig. 4(b) showing a large semiclassical R. Figure 5(a) shows that R becomes very large for $T=7.4°$ around $\theta=140°$. Figure 5(b) shows that this near divergence is not due to a large negative imaginary part of F, since $\mathrm{Im}(F)$ remains positive both at $T=7.0$ and at $T=7.4$. Figure 5(c) shows the prefactor of the semiclassical propagator $|\det(M_{\mathbf{vv}})|^{-1/2}$, which indeed becomes very large for $T=7.4$. Notice that there are two contributions at $\theta=140$ (two square symbols in the figure), corresponding to two different trajectories satisfying the same boundary conditions. The family of one of these trajectories contributes alone for $\theta<140$ whereas the other family contributes alone for $\theta>140$. This is clearly seen in Fig. 5(d), which shows the phase of the prefactor. For $T=7.4$, the phase jumps by π at $\theta=140$, exactly as in the case of caustics in the usual coordinate representation.

Figure 5 suggests strongly that the large values of the semiclassical return probability in Fig. 4(b) are due to caustics. To demonstrate that this is indeed the case, we show the bifurcation explicitly in Fig. 6. Panel (a) shows the return probability at $x=0.72$, $y=0.24$, $E=0.5$, and $\theta=140°$ as a function of T, showing again the peak at $T=7.4$. Panels (b)–

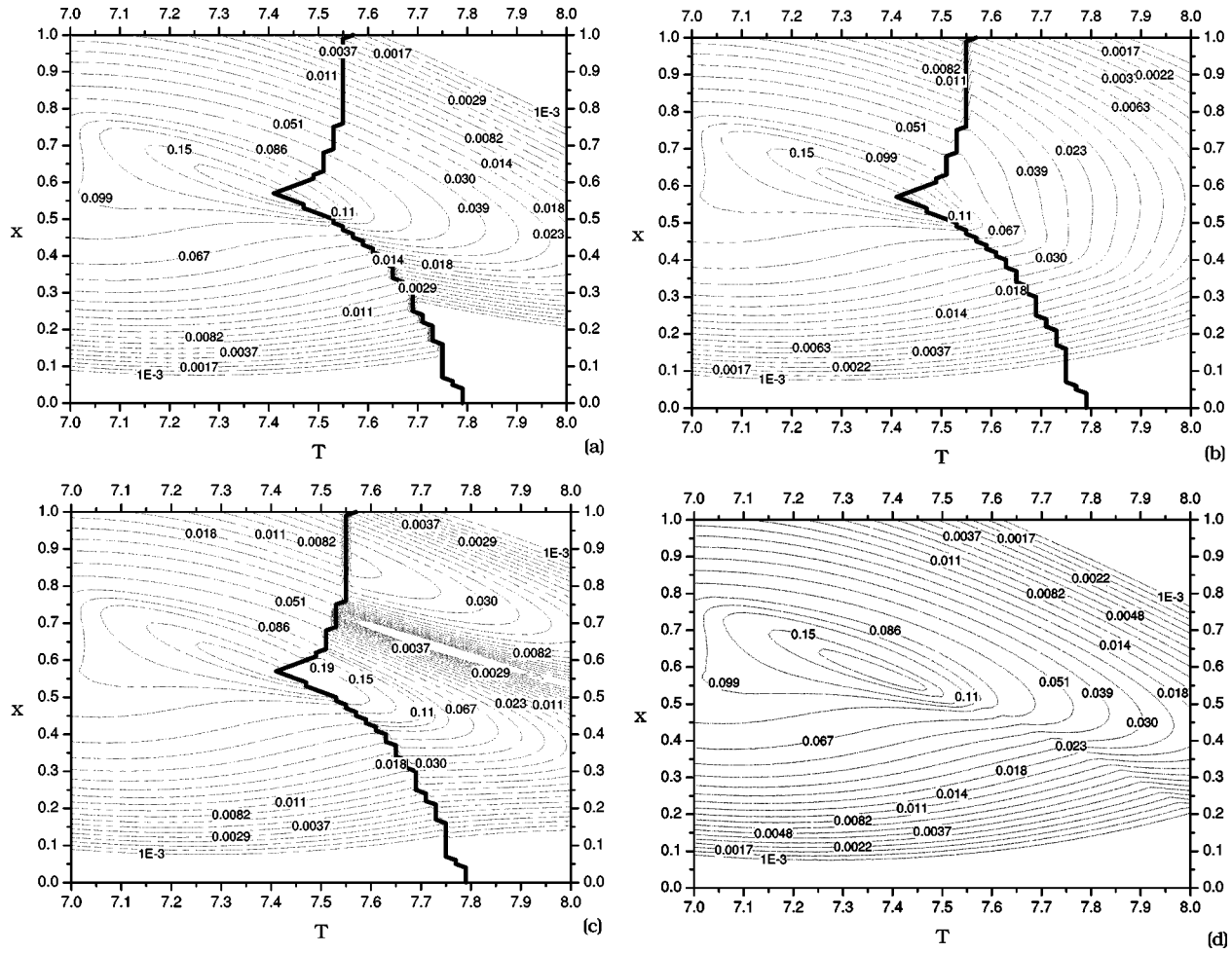

FIG. 7. Semiclassical return probability in the Tx plane for $\theta=140$, $y=3x/2$ and $E=0.5$. The peak at $T\approx 7.4$, $x\approx 0.55$ is the bifurcation point. To the right of the gray lines two trajectories exist. The first trajectory is continuous as it crosses the upper gray line and discontinuous at the lower gray line, and vice versa for the second trajectory. (a) Contribution of one the trajectories, (b) contribution of the other trajectory, (c) both contributions are taken into account, (d) at each point only one of the two trajectories contribute, according to the Stokes line criterion.

(d) show a detailed analysis of the contributing trajectories as a function of T. For $T<7.4$ we find a single complex trajectory satisfying the boundary conditions, whereas two such trajectories are found for $T\geqslant 7.4$. The new trajectory bifurcates from that existing for $T<7.4$. Their separate contributions to the propagator are shown in panel (b). Panel (c) shows the imaginary part of F and panel (d) shows the prefactor. This bifurcation is probably connected to the bifurcation of the asymmetric families of periodic orbits from the symmetric family [26], which occurs at $E\approx 0.38$ when the period of the orbits is $T\approx 7.55$. The detailed connection between the periodic orbits bifurcation and the complex trajectories bifurcation deserves a deeper understanding, and will be the object of future research.

Notice that, for fixed initial conditions x, y, θ, and E, the solutions of Hamilton's equations satisfying $\mathbf{z}'=\mathbf{z}$ and $\mathbf{z}''^{*}=\mathbf{z}^{*}$ form one-parameter families, parametrized by T. In each plot showing the return probability, E and T are fixed. Therefore, if we find values x_0, y_0, and θ_0 where one of the eigenvalues of $M_{\mathbf{vv}}$, λ, is zero, then the dimensionality of the set of singular points, where $\lambda=0$, can be obtained by setting $\delta\lambda=a\delta x+b\delta y+c\delta\theta=0$, where a, b, and c are derivatives of λ with respect to x, y, and θ calculated at x_0, y_0, θ_0. Since the coefficients a, b, and c are complex, the equation $\delta\lambda=0$ can be solved in terms of $\delta\theta$ to give $\delta x=\delta x(\delta\theta)$ and $\delta y=\delta y(\delta\theta)$. This means that the singular set, where the bifurcation occurs, forms a one-dimensional curve in the x,y, θ space. This is compatible with the semiclassical plots shown in Fig. 4. Actually, since our grids in the xy plane and in the angle θ are rather coarse, we never hit the very bifurcation point, but we may pass close to it.

Going back to the semiclassical return probability plot for $T=7.4$, Fig. 4(c) shows the result with the contributions of all $xy\theta$ points near such bifurcations removed. Comparing this figure with the exact return probability, Fig. 3 for $T=7.4$, we find very good agreement.

D. Stokes lines

Finally we discuss the last, and perhaps most difficult, question. After a bifurcation, and sufficiently far from the bifurcation point, two (or more) trajectories may contribute

similar amounts to the return probability. Figure 6(b) for $T \gtrsim 7.5$ shows an example of this situation where two trajectories exist. Should both contributions be included in the semiclassical formula?

In order to understand the situation, we plot in Figs. 7(a) and 7(b) contour levels of the semiclassical return probability calculated along the line $y=2x/3$, $0 \leqslant x \leqslant 1$, for a fixed angle $\theta=\theta_0=140$, $E=0.5$, and for $7.0 \leqslant T \leqslant 8.0$. This line crosses the bifurcation region in Fig. 4(b). The bifurcation shows itself in Fig. 7 as a peak close to $T=7.4$, $x=0.55$. For $\theta \neq \theta_0$ the bifurcation occurs at different points in the Tx plane. The two gray lines emanating from the bifurcation point show the projection on this plane of the bifurcations at other angles. On the left of the gray lines there is a single trajectory satisfying the boundary conditions. On the right of the gray lines there are two such trajectories. Notice that there is no divergence as we cross these lines away from the central peak: since the bifurcation is not exactly there, the two trajectories on the right side of the line are different from each other, and not infinitesimally similar as in the case of a bifurcation.

Figure 7(a) shows the return probability computed with only one of these trajectories. Figure 7(b) shows the same thing but using only the other trajectory. The regions where each trajectory exists form superimposed sheets in the Tx plane.

If the two trajectories on the right of the gray lines are included in the semiclassical formula, the approximation becomes clearly discontinuous, as shown by Fig. 7(c). Notice that the family of trajectories in Fig. 7(a) produces continuous results when the upper gray line is crossed, while the family in Fig. 7(b) produces continuous results when the lower gray is crossed. This suggests that there is a line emanating from the bifurcation point (and between the two gray lines) which separates the region where each family contributes alone. This line can be found by demanding the approximation to be continuous: it is the Stokes line for this problem. The result of this division, shown in Fig. 7(d), is a smooth and continuous semiclassical picture. The division line can actually be seen (approximately) in Figs. 7(a) and 7(b) as the place where the contour lines change curvature quite suddenly.

Notice that the upper critical line radiating from the bifurcation point in Fig. 7 ends vertically at $T \approx 7.55$. This is exactly the bifurcation period of the symmetric family into the asymmetric ones, pointing again to a connection between the periodic orbits and complex orbits bifurcations.

Although the analysis above elucidates the interplay between trajectories after a bifurcation, it does not point to a simple and direct way to decide which of them should be included when one is plotting R, as in Fig. 4. However, it turns out that the right choice of trajectory can be made automatically by feeding the search algorithm with the starting real periodic orbit which is closest (in phase space) to the point where the return probability is being evaluated. For the range of periods studied here, this simple procedure worked very well.

As an example we show in Fig. 8(a) the return probability for $T=7.7$ calculated adding the two contributions that appear after the bifurcation at 7.4. Figure 8(b) shows the same

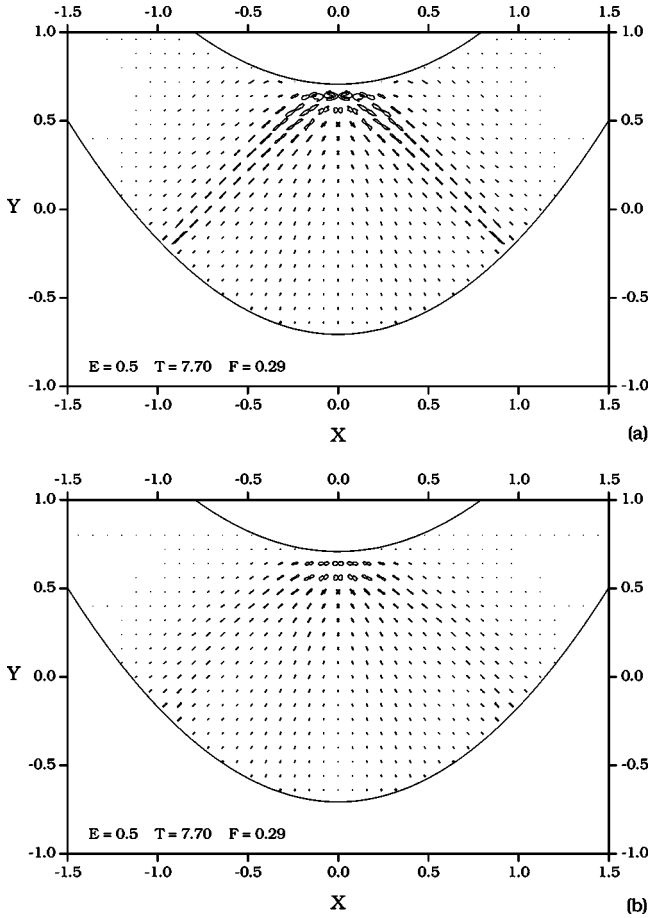

FIG. 8. Semiclassical return probability for $T=7.7$ with (a) the two contributions after the bifurcation and (b) with a single contribution.

calculation taking into account only the contribution whose initial seed is the closest real periodic orbit. This gives a very good result if compared to the exact quantum calculation in Fig. 3.

E. Filtered results

Figure 9 shows the semiclassical return probability for the same values of T shown in Fig. 2, close to the period of the shortest periodic orbit. In this region, although no bifurcations exist, we do find a few noncontributing trajectories, whose actions have negative imaginary parts. When these are filtered out, the semiclassical result becomes very similar to the exact quantum mechanical calculations Fig. 2.

Figure 10 shows the semiclassical calculations for the same values of T shown in Fig. 3. This time not only noncontributing trajectories had to be filtered out but also several trajectories close to caustics had to be eliminated. At these points we have simply not computed the propagator at all. This is responsible for the kinky plots around some x,y points. It is, however, very interesting to see how the plot for $T=7.7$ reproduces faithfully the quantum mechanical results, displaying a structure similar to the symmetric periodic orbit of Fig. 1(a). Notice, however, that the symmetric orbit has the period 7.1, while this structure shows up at 7.7. Therefore

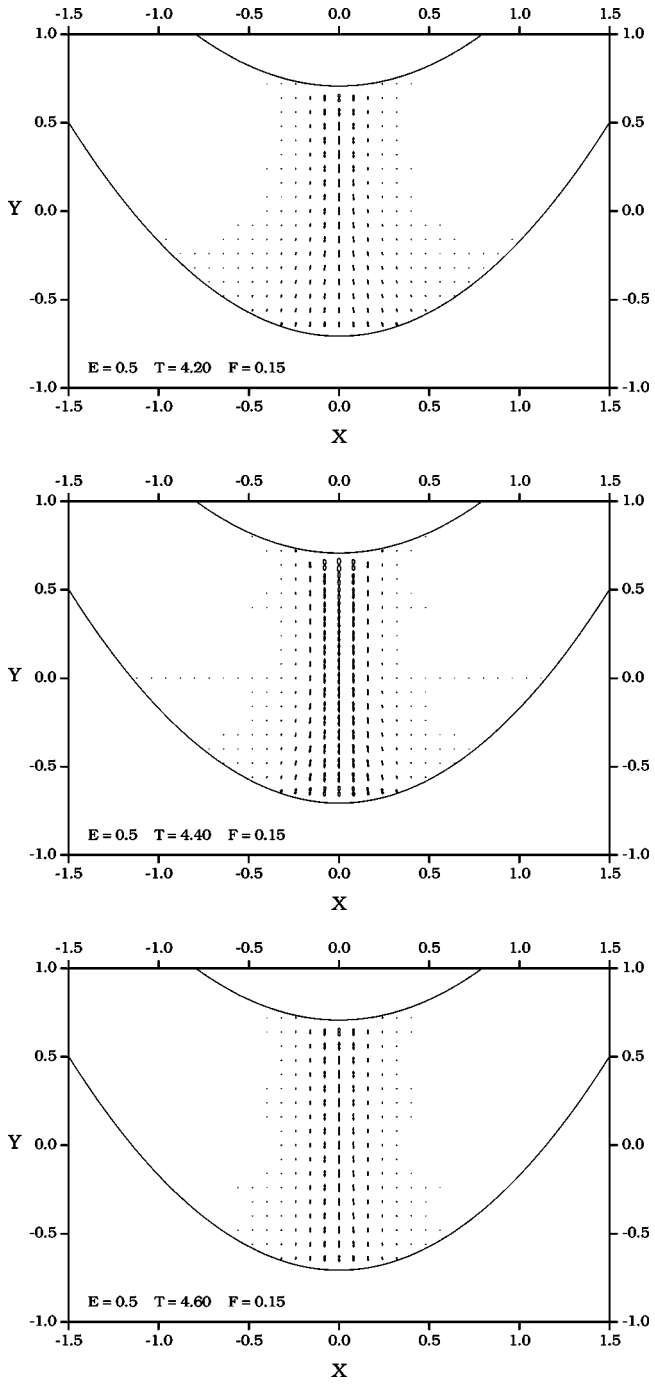

FIG. 9. Semiclassical return probability with noncontributing trajectories filtered out for $T=4.2$, 4.4, and 4.6.

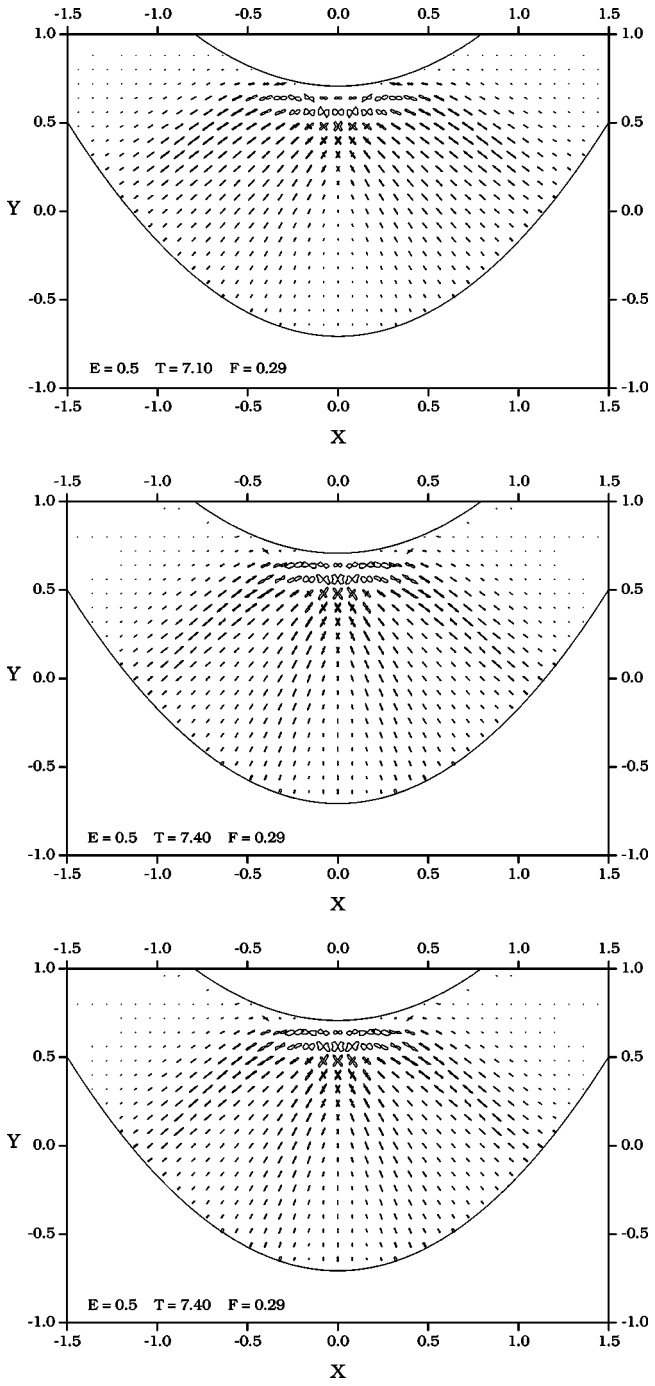

FIG. 10. Semiclassical return probability with noncontributing trajectories filtered out and points close to caustics removed for $T=7.1$, 7.4, and 7.7.

it does not correspond to a real periodic orbit of the Nelson potential. This shows the importance of complex trajectories in the semiclassical coherent state propagator.

VII. CONCLUSIONS

We have compared exact and semiclassical coherent state propagators for a soft chaotic system with two degrees of freedom. The semiclassical calculation relies on classical complex trajectories of a smoothed Hamiltonian satisfying specific boundary conditions. Not all these trajectories, however, contribute to the propagator.

The reasons why a trajectory might not contribute can be understood if one bases the semiclassical approximation on the steepest descent method. This is a powerful and very useful tool in semiclassical analysis. It replaces the integration of oscillatory functions by the stationary phase method, in which the integrand is replaced by Gaussians centered on the saddle points of its phase. However, in the steepest descent method, it is well known that not all saddle points

contribute to the asymptotic approximation: one has to be able to deform the original contour of integration into that passing through the steepest descent path of the saddle. The Airy function is a well studied example of this problem.

In the case of path integrals, the question of contributing points becomes more involved because of the infinite number of integrals to which the approximation is applied. The saddle point is replaced by a saddle "curve" and identifying which of them should contribute or not to the semiclassical formula from a topological point of view is very hard. Therefore, instead of relying on rigorous mathematical criteria, we appeal to physical arguments. One of these arguments is the magnitude of the contribution itself. Many of the complex classical trajectories found by our search method have actions whose imaginary part is negative. Some of these trajectories alone give contributions that result in $|K(\mathbf{z},\mathbf{z},T)|>1$, which is clearly unphysical. These trajectories are therefore eliminated.

The other situation has to do with the aftermath of caustics. When computing the return probability for a fixed time T and energy $E=H(\mathbf{z})$, we found regions where two trajectories (both with positive imaginary parts of the action) exist. The regions where each of these families of trajectories are found form sheets that meet at a bifurcation point. In the regions where these sheets are superimposed one cannot consider the contributions from both trajectories, since that would render the propagator discontinuous. To avoid this problem we take only one of the trajectories, following its sheet from the region where it exists alone into the region where its sheet meets that of the other family. When the magnitude of its contribution equals that of the other family, we switch sheets. This procedure guarantees continuity of the semiclassical result and turns out to produce excellent agreement with the exact calculations.

ACKNOWLEDGMENTS

M.A.M.A. and A.D.R. acknowledge financial support from CNPq, FAPESP, and FINEP. A.D.R. especially acknowledges FAPESP for Grant No. 00/00063-2.

[1] J. R. Klauder, *Path Integrals*, edited by G. J. Papadopoulos and J. T. Devreese, *NATO Advanced Study Institute, Series B: Physics* (Plenum, New York, 1978).
[2] J. R. Klauder, Phys. Rev. D **19**, 2349 (1979).
[3] J. R. Klauder, in *Random Media*, edited by G. Papanicolaou (Springer, Berlin, 1987).
[4] Y. Weissman, J. Chem. Phys. **76**, 4067 (1982).
[5] M. Baranger, M. A. M. de Aguiar, F. Keck, H. J. Korsch, and B. Schellaaß, J. Phys. A **34**, 7227 (2001).
[6] J. R. Klauder and B. S. Skagerstam, *Coherent States, Applications in Physics and Mathematical Physics* (World Scientific, Singapore, 1985).
[7] S. Adachi, Ann. Phys. (N.Y.) **195**, 45 (1989).
[8] J. R. Klauder, Phys. Rev. Lett. **56**, 897 (1986).
[9] J. R. Klauder, Ann. Phys. (N.Y.) **180**, 108 (1987).
[10] A. Rubin and J. R. Klauder, Ann. Phys. (N.Y.) **241**, 212 (1995).
[11] A. Tanaka, Phys. Rev. Lett. **80**, 1414 (1998).
[12] A. L. Xavier, Jr. and M. A. M. de Aguiar, Ann. Phys. (N.Y.) **252**, 458 (1996).
[13] A. L. Xavier, Jr. and M. A. M. de Aguiar, Phys. Rev. A **54**, 1808 (1996).
[14] A. L. Xavier, Jr. and M. A. M. de Aguiar, Phys. Rev. Lett. **79**, 3323 (1997).
[15] F. Grossmann, Phys. Rev. A **57**, 3256 (1998).
[16] T. Van Voorhis and Eric J. Heller, Phys. Rev. A **66**, 050501 (2002).
[17] T. Van Voorhis and Eric J. Heller, J. Chem. Phys. **119**, 12 153 (2003).
[18] R. S. Kaushal and H. J. Korsch, Phys. Lett. A **276**, 47 (2000).
[19] R. S. Kaushal and Shweta Singh, Ann. Phys. (N.Y.) **288**, 253 (2001).
[20] M. C. Gutzwiller, J. Math. Phys. **12**, 343 (1971).
[21] E. Bogomolny, Physica D **31**, 169 (1988).
[22] D. Provost and M. Baranger, Phys. Rev. Lett. **71**, 662 (1993).
[23] M. Baranger, M. Hagerty, B. Lauritzen, D. C. Meredith, and D. Provost, Chaos **5**, 261 (1995).
[24] M. Baranger and M. A. M. de Aguiar (unpublished).
[25] M. Baranger, K. T. R. Davies, and J. H. Mahoney, Ann. Phys. (N.Y.) **186**, 95 (1988).
[26] M. Baranger and K. T. R. Davies, Ann. Phys. (N.Y.) **177**, 330 (1987).
[27] M. A. M. de Aguiar, C. P. Malta, M. Baranger, and K. T. R. Davies, Ann. Phys. (N.Y.) **180**, 167 (1987).
[28] D. Provost and P. Brumer, Phys. Rev. Lett. **74**, 250 (1995).
[29] D. Provost, Phys. Rev. E **51**, 5396 (1995).